

## ARTICLE

# The role of GTF2IRD1 in the auditory pathology of Williams–Beuren Syndrome

Cesar P Canales<sup>1</sup>, Ann CY Wong<sup>2</sup>, Peter W Gunning<sup>1</sup>, Gary D Housley<sup>2</sup>, Edna C Hardeman<sup>1</sup> and Stephen J Palmer<sup>\*,1</sup>

Williams–Beuren Syndrome (WBS) is a rare genetic condition caused by a hemizygous deletion involving up to 28 genes within chromosome 7q11.23. Among the spectrum of physical and neurological defects in WBS, it is common to find a distinctive response to sound stimuli that includes extreme adverse reactions to loud, or sudden sounds and a fascination with certain sounds that may manifest as strengths in musical ability. However, hearing tests indicate that sensorineural hearing loss (SNHL) is frequently found in WBS patients. The functional and genetic basis of this unusual auditory phenotype is currently unknown. Here, we investigated the potential involvement of GTF2IRD1, a transcription factor encoded by a gene located within the WBS deletion that has been implicated as a contributor to the WBS assorted neurocognitive profile and craniofacial abnormalities. Using *Gtf2ird1* knockout mice, we have analysed the expression of the gene in the inner ear and examined hearing capacity by evaluating the auditory brainstem response (ABR) and the distortion product of otoacoustic emissions (DPOAE). Our results show that *Gtf2ird1* is expressed in a number of cell types within the cochlea, and *Gtf2ird1* null mice showed higher auditory thresholds (hypoacusis) in both ABR and DPOAE hearing assessments. These data indicate that the principal hearing deficit in the mice can be traced to impairments in the amplification process mediated by the outer hair cells and suggests that similar mechanisms may underpin the SNHL experienced by WBS patients.

*European Journal of Human Genetics* (2015) 23, 774–780; doi:10.1038/ejhg.2014.188; published online 24 September 2014

## INTRODUCTION

Williams–Beuren Syndrome (WBS) is a complex neurodevelopmental condition characterised by multiple physical and neurological abnormalities with an estimated incidence of 1 in 7500.<sup>1</sup> WBS is usually caused by a 1.5–1.8 Mb hemizygous deletion containing up to 28 genes within chromosome 7q11.23.<sup>2</sup> The clinical presentation of the neurological features includes mild to moderate intellectual disability, a characteristic visuospatial construction deficit and abnormal motor coordination. In addition, patients have a highly distinctive personality profile that includes ‘over-friendliness’ because of a lack of normal social inhibition and enhanced emotional empathy, but this is combined with heightened anxiety in response to non-social cues leading to high rates of phobias.<sup>3</sup>

Genotype–phenotype correlations drawn from patients who carry atypical deletions within the region suggest that haploinsufficiency of gene products from *GTF2IRD1* and *GTF2I* account for the major aspects of the WBS neurocognitive profile.<sup>4</sup> *GTF2I* and *GTF2IRD1* are evolutionarily related and encode homologous proteins (TFII-I and GTF2IRD1) that are thought to act as multi-functional transcription factors. Evidence indicates that TFII-I and GTF2IRD1 have overlapping properties, can physically interact with each other and share a similar range of target genes.<sup>5–7</sup> In addition, work on mice carrying mutations of the orthologous genes *Gtf2i* and *Gtf2ird1* supports a role for these genes in the craniofacial and neurological features of WBS. In particular, homozygous null *Gtf2ird1* mouse mutant lines show abnormal craniofacial development, altered anxiety responses in social and non-social

contexts, altered exploratory drive and increased vocalisation in response to stressful stimuli and impaired motor coordination.<sup>8–11</sup>

One of the typical features of WBS is an abnormal hearing response, classically described as ‘hyperacusis’. This term aims to describe the extreme adverse behavioural reactions of WBS patients to sounds that are not normally regarded as loud or aversive and are generally acceptable to others. However, use of the term is inaccurate because hyperacusis implies increased functional sensitivity leading to detectably lower hearing thresholds.<sup>12</sup> Auditory allodynia, meaning aversion to, or fear of certain sounds that are usually acceptable to others, is a more accurate description of this condition.<sup>12</sup>

Several studies have shown that WBS patients of all ages show increased rates of mild to moderate high-frequency sensorineural hearing loss (SNHL).<sup>13–15</sup> SNHL in WBS has been shown to be progressive and the prevalence may develop to ~80% of subjects over time.<sup>16</sup> Although many younger WBS patients seem to have hearing in the normal range, it is generally agreed that analysis of otoacoustic emissions from the cochlea of these patients indicates high rates of abnormalities,<sup>15–18</sup> suggesting a degree of ‘cochlear fragility’,<sup>15</sup> associated with altered sound transduction. Measurement of the distortion product of otoacoustic emissions (DPOAEs) is a non-invasive, highly sensitive, objective measure of the cochlear amplifier mechanism mediated by the outer hair cells. Thus, rates of SNHL may be low in young WBS individuals but most show evidence of incipient cochlear dysfunction and will later go on to develop SNHL, particularly in the high-frequency range.<sup>16</sup>

<sup>1</sup>Cellular and Genetic Medicine Unit, School of Medical Sciences, UNSW Australia, Sydney, NSW, Australia; <sup>2</sup>Translational Neuroscience Facility, Department of Physiology, School of Medical Sciences, UNSW Australia, Sydney, NSW, Australia

\*Correspondence: Dr SJ Palmer, Department of Anatomy, School of Medical Sciences, Room 234, Wallace Wurth (C27), UNSW Australia, Sydney, NSW 2052, Australia. Tel: +61 2 9385 2957; Fax: +61 2 9385 0022; E-mail: s.palmer@unsw.edu.au

Received 19 February 2014; revised 11 August 2014; accepted 15 August 2014; published online 24 September 2014

The cause of the auditory pathology in WBS is currently unknown and has led some to speculate on a possible contribution from the observed effects of premature ageing and/or a high predisposition for noise-induced cochlear damage that could be connected to the so-called hyperacusis.<sup>17</sup> Involvement of the haploinsufficiency of elastin due to hemizygous loss of the *ELN* gene is a popular hypothesis<sup>15,17,18</sup> because of its profound impact on other organ systems and expression of the gene in several key hearing structures. Loss of the *LIMK1* gene has also been implicated as it encodes a kinase that regulates actin reorganisation and has a role in the control of outer hair cell motility.<sup>19</sup> Further examples of potential altered gene expression associated with WBS include *FZD9*, which is expressed in adult spiral ganglion neurons<sup>20</sup> and *STX1A*, which is expressed in the inner and outer hair cells.<sup>21</sup> Although it is possible that any of these genes could contribute to the WBS hearing phenotype, such hypotheses have not yet been tested.

In this study, we aimed to examine a possible role for the GTF2IRD1 protein in the auditory pathology of WBS by examining *Gtf2ird1* knockout mice. However, acoustic tests in mice usually rely on behavioural responses, such as noise-evoked freezing time, and could be confounded by the altered anxiety responses previously reported in *Gtf2ird1* knockouts.<sup>8,11</sup> In heterozygous *Gtf2i* mutant mice, 'hyperacusis' was reported on the basis of a mild increase in freezing response time. In addition, the mice also showed increased anxiety in the elevated plus maze and light-dark box tests.<sup>22</sup> To obviate any potential confounds between these phenotypes, we chose to use the objective physiological measures of auditory brainstem response (ABR) and DPOAE, which are conducted under general anaesthesia and therefore have a minimal behavioural component. Both of these assays showed that *Gtf2ird1* knockout mice have a significant loss in hearing sensitivity and the DPOAE data indicate that this can be attributed to a dysfunction of the cochlear amplifier. We confirmed that *Gtf2ird1* is expressed in the sensorineural tissues of the *Gtf2ird1<sup>tm2(LacZ)Hrd</sup>* mouse cochlea, including the auditory receptor outer hair cells. We propose, on this basis, that loss of GTF2IRD1 has an important role in the auditory pathology of WBS mediated via a dysfunction of the cochlear amplifier.

## MATERIALS AND METHODS

### Mice

The *Gtf2ird1<sup>tm1Hrd</sup>* and *Gtf2ird1<sup>tm2(LacZ)Hrd</sup>* mouse models and genotyping methods were described previously.<sup>23,24</sup> Both lines were maintained on a C57BL/6J background and homozygous *Gtf2ird1<sup>tm1Hrd</sup>* and wild-type siblings were produced in the same litters from heterozygous parents and housed together in identical conditions. The *Gtf2ird1<sup>tm1Hrd</sup>* line was used to assess hearing capacity and heterozygous and homozygous mutant mice are hereinafter referred to as *Gtf2ird1<sup>-/+</sup>* and *Gtf2ird1<sup>-/-</sup>*, respectively. Mice were 8- to 10-week old at the time of hearing testing by ABR and DPOAE. All experimental procedures were approved by the Animal Care and Ethics Committee at UNSW Australia.

### Immunofluorescence analysis of *Gtf2ird1* expression in the cochlea

Mice were anaesthetised and transcardially perfused with cold 0.1 M phosphate-buffered saline and cold 4% paraformaldehyde (PFA). Tympanic bullae containing the cochleae were dissected under the microscope and locally perfused with 4% PFA through the round and oval windows. Samples were kept in 4% PFA at 4 °C overnight and then decalcified in 8% EDTA in 0.1 M phosphate buffer (PB, pH 7.4) for 2 weeks at 4 °C. Decalcified cochleae were rinsed in PB, transferred to a 30% sucrose solution for incubation overnight and then transferred to a 1:1 mixture of 30% sucrose and OCT compound (TissueTek, Sakura Finetek Inc., Torrance, CA, USA) for 4 h before being snap-frozen in OCT using liquid nitrogen.

Immunofluorescence analysis was performed using 30 µm floating cryosections in 24-well plates (Nalgen Nunc Int., Rochester, NY, USA) containing PB. Sections were permeabilized for 1 h with 1% Triton X-100 in PB and blocked with 5% normal goat serum and 5% bovine serum albumin in PB. The primary anti-β-galactosidase antibody (Molecular Probes, Eugene, OR, USA; cat# 08633651) was diluted 1:500 in blocking solution and applied overnight at 4 °C. In control experiments, the primary antibody was omitted. Sections were washed three times with PB containing 0.2% Triton X-100, followed by 1 h incubation in the secondary antibody solution containing goat anti-rabbit Alexa Fluor 488 (Molecular Probes) at 1:1000 in PB. Sections were washed three times with PB and mounted with ProLong Gold Antifade Reagent containing DAPI (Molecular Probes, cat# P-36931). Images were captured using a confocal microscope (Zeiss, Oberkochen, Germany; T710). Similarly, spiral ganglion neuronal labelling was undertaken using rabbit anti-bovine neurofilament 200 immunofluorescence (Sigma-Aldrich, Castle Hill, NSW, Australia; N4142; 1:1000), with detection using Alexa Fluor 488 goat anti-rabbit IgG (1:1000). F-actin labelling was achieved by incubating the permeabilized tissue with Alexa Fluor 594-phalloidin (1:250).

### ABR

ABR was evaluated in *Gtf2ird1<sup>-/-</sup>*, *Gtf2ird1<sup>-/+</sup>* and wild-type littermates at the age of 8–10 weeks. All ABR measurements were performed in a sound attenuating chamber (Sonora Technology, Shizuoka, Japan). Mice were anaesthetised with a cocktail of ketamine (40 mg/kg), xylazine (8 mg/kg) and acepromazine (0.5 mg/kg). Supplemental doses of K/X/A cocktail were given as necessary throughout the experiments (typically after 30 min). Body temperature was maintained using a heating pad regulated via a rectal probe and ophthalmic ointment was applied to the eyes of the animal to prevent corneal drying. ABRs were recorded by placing fine platinum subdermal electrodes at the mastoid region of the right ear (active electrode), scalp vertex (reference electrode) and on the lower back (ground electrode). The acoustic stimuli for ABR were produced and responses recorded using a Tucker-Davis Technologies auditory physiology System III workstation (TDT, Fort Lauderdale, FL, USA), controlled by BIOSIG32 software (Ver. 4.1.1; TDT). ABR potentials were evoked with digitally produced 5 ms tone pips (0.5 ms rise/fall time, delivered at 10/s) delivered by an electrostatic speaker (EC1; TDT). Signal recordings (10 ms duration) in response to broadband click (100 µs) or tone pip (4, 8, 16, 24 and 32 kHz) sound stimuli were amplified, filtered and averaged up to 512 times. For each sound stimulus, sound pressure level (SPL) signals were decreased in 5 dB steps, starting from 70 dB, down to 10 dB below the threshold level. The intensity at which an ABR complex (waves I–V) was no longer distinguishable from the noise floor (200 nV peak-to-peak) was defined as the ABR threshold. All response values (thresholds, peak to peak amplitudes and latencies) were determined by off-line analysis. Speaker calibration was carried out using a calibrating microphone connected to the TDT system via its companion preamplifier (Aco Pacific, Belmont, CA, USA), with SIGCALRP and RPVDSEX software (TDT).

### Distortion product otoacoustic emissions

The cubic distortion product otoacoustic emissions (DPOAE at  $2f_1-f_2$ ) were recorded using a custom-made ear canal probe containing a microphone (ER-B10+, Etymotic Research, Elk Grove Village, IL, USA). Two EC1 speakers delivered the primary tones ( $f_1$  and  $f_2$ ;  $f_2/f_1$  ratio = 1.25) of 8, 12, 16, 24 and 32 kHz (168 ms duration, 6/s from 0 to 80 dB in 5 dB increments) within this acoustic coupler. The  $f_1$  and  $f_2$  amplitudes were equivalent. The auditory canal signals were analysed by fast Fourier transformation with 50 traces per sound level being averaged. The DPOAE threshold for a specific tonal level was defined as the lowest SPL at which a  $2f_1-f_2$  DPOAE was detectable above noise floor.

### Statistical data analysis

Results are presented as the mean ± SEM, and statistical analysis was performed using two-way repeated measures analysis of variance on ranks (Holm-Sidak method; Sigmaplot, Systat Software Inc., San Jose, CA, USA) with confirmation of normal distribution of the data. Significance was determined as  $P < 0.05$ .

## RESULTS

### Expression of *Gtf2ird1* in the cochlea

Detection of nuclear-localised  $\beta$ -galactosidase in heterozygous *Gtf2ird1*<sup>tm2(LacZ)Hrd</sup> knock-in mice was used as a sensitive means to map the normal expression of *Gtf2ird1* transcript<sup>24</sup> in the adult cochlea (Figure 1). Although the harsh decalcification methods required for sectioning make the usual histochemical  $\beta$ -galactosidase detection method impossible, indirect-immunofluorescence detection of  $\beta$ -galactosidase showed clear signals in the nuclei of several cell types and also some background immunofluorescence, mainly associated with the remaining extracellular matrix of the bone tissue. This could be easily distinguished from the real signal by the lack of nuclear localisation and by comparison with control cochlea sections from wild-type mice treated identically (Figure 1c). *Gtf2ird1* expression was identified in the epithelial cell layer of Reissner's membrane, interdental cells, marginal cells of the stria vascularis and the spiral ganglion neurons of the cochlear nerve. Expression was also detected in the auditory sensory receptor inner and outer hair cells, inner and outer pillar cells, Deiters' cells, Boettcher cells and Hensen's cells (Figure 1).

### Structure of the *Gtf2ird1* knockout cochlea

The structure of the *Gtf2ird1*<sup>-/-</sup> cochlea tissue showed no evidence of morphological impact from lack of the GTF2IRD1 protein (Figures 2a and b). Fluorescent rhodamine phalloidin labelling of the f-actin in the hair cells within whole mounts of the organ of Corti from WT and KO mice were examined (two each). Qualitative comparisons showed no

discernible difference in hair cell density in the regions examined (mid to basal turn; Figure 2c).

### *Gtf2ird1* knockout mice have a hearing deficit across a broad frequency range

Hearing function was assessed in a cohort of *Gtf2ird1*<sup>-/-</sup>, *Gtf2ird1*<sup>-/+</sup> and wild-type littermates ( $n = 15$  for each genotype) by ABR. Sound-evoked ABR recordings reflect synchronous activation of elements of the brainstem auditory pathway, from the cochlear nerve, through the cochlear nucleus, superior olivary complex, medial nucleus of the trapezoid body, lateral lemniscus and inferior colliculus, manifested as four or five distinctive temporally synchronised peaks (Figure 3a and b).<sup>25</sup> The ABR waveforms were similar for *Gtf2ird1*<sup>-/-</sup>, *Gtf2ird1*<sup>-/+</sup> and wild-type mice. In response to click stimuli (broadband), *Gtf2ird1*<sup>-/-</sup> mice manifested a 6.7 dB increase in hearing threshold compared with their wild-type littermates (wild type =  $25.5 \pm 1.10$  dB; *Gtf2ird1*<sup>-/-</sup> =  $32.2 \pm 3.03$  dB;  $P = 0.047$ ). At 4 kHz, the *Gtf2ird1*<sup>-/-</sup> mice showed a 10.2-dB increase in threshold (wild type =  $26.7 \pm 0.90$ ; *Gtf2ird1*<sup>-/-</sup> =  $36.8 \pm 3.38$ ;  $P = 0.007$ ). The average difference in hearing threshold between 8 and 32 kHz was 6.4 dB (average increase in ABR threshold in *Gtf2ird1*<sup>-/-</sup> mice: 8 kHz = 7.53 dB; 16 kHz = 4.00 dB; 24 kHz = 6.67 dB; 32 kHz = 7.33 dB) revealing a mild hearing deficit across the range of test frequencies (Figures 3b and c). No differences in threshold were detected in *Gtf2ird1*<sup>-/+</sup> mice when compared with wild-type littermates ( $n = 15$ ; for wild type, *Gtf2ird1*<sup>-/+</sup> and *Gtf2ird1*<sup>-/-</sup> mice;  $P < 0.001$  via 2 way ANOVA on ranks when comparing *Gtf2ird1*<sup>-/-</sup> with wild type).

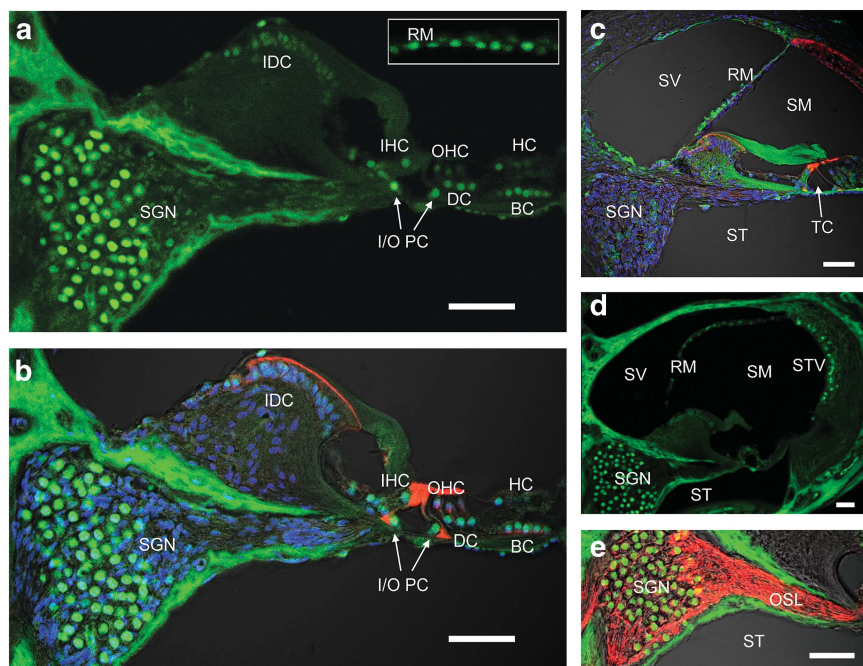


**Figure 1** *Gtf2ird1* expression in the adult *Gtf2ird1*<sup>tm2(LacZ)Hrd</sup> mouse cochlea. (a)  $\beta$ -Galactosidase nuclear immunofluorescence (representing *Gtf2ird1* expression) was present in the sound transducing inner hair cells (IHCs) and outer hair cells (OHCs). Expression of *Gtf2ird1* was also detected in the inner and outer pillar cells (I/O PCs), Deiters' cells (DCs), cells of Boettcher (BCs), interdental cells (IDCs) and Hensen's cells (HCs). A more intense level of immunofluorescence was seen in the spiral ganglion neurons (SGNs). Inset shows expression of *Gtf2ird1* in epithelial cells of Reissner's membrane (RM). (b) The same image overlaid with phalloidin staining (red) of actin filaments, which identifies the IHCs and OHCs, and DAPI (blue), which shows the location of all cell nuclei. (c) Control cochlea section from a wild-type mouse showing phalloidin, DAPI and the extent of green fluorescence background with the  $\beta$ -galactosidase antibody, but no specific signal was observed in cell nuclei (SM, scala media; ST, scala tympani; SV, scala vestibuli; TC, tunnel of Corti). (d) Low-magnification immunofluorescence image of cochlear section from a *Gtf2ird1*<sup>tm2(LacZ)Hrd</sup> mouse showing *Gtf2ird1* expression in the marginal cells of the stria vascularis (STV). (e) Detailed *Gtf2ird1* expression in the afferent auditory SGN that project to the hair cells of the organ of Corti via the osseous spiral lamina (OSL), identified using neurofilament 200 antibody (red). Panels b, c and e also include merged transmitted light images to highlight cochlear morphology. Scale bars, 50  $\mu$ m.



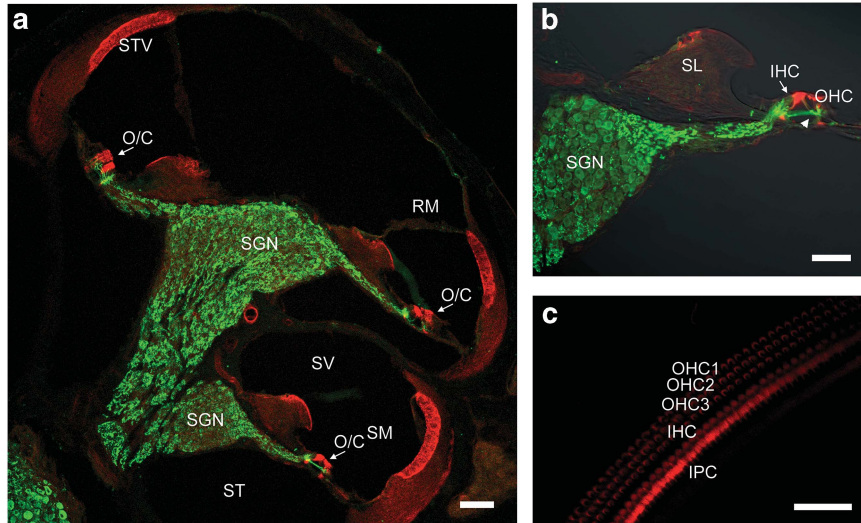


**Figure 2** Histology of *Gtf2ird1*<sup>-/-</sup> cochlea confirms normal cytoarchitecture. (a) Representative low-power image of a *Gtf2ird1*<sup>-/-</sup> mouse cochlear mid-modiolar cryosection showing the innervation labelled with Neurofilament 200 immunofluorescence (green) and the organ of Corti (O/C) and structural tissues labelled for filamentous actin with Alexa Fluor 594-phalloidin fluorescence (red). White arrows indicate O/C, where the sensory hair cells and supporting cells were strongly labelled for f-actin. RM, Reissner's membrane; SGN, spiral ganglion; SM, scala media; ST, scala tympani; STV, stria vascularis; SV, scala vestibuli. Scale bar, 100  $\mu$ m. (b) Detail of the structural integrity of the O/C and SGN. Arrow-head indicates olivocochlear efferent innervation of the outer hair cells (OHCs). Arrow indicates afferent innervation of the inner hair cells. IHC, inner hair cell; S, spiral limbus. Image includes transillumination for structural detail. Scale bar, 50  $\mu$ m. (c) Surface-mount, mid-basal turn O/C with Alexa Fluor 594-phalloidin fluorescence confirms the integrity of the three rows of OHCs (1–3) and single row of IHCs supported by corresponding inner phalangeal cells (IPCs). Labelling of the hair cell stereocilia was prominent. Scale bar, 50  $\mu$ m.

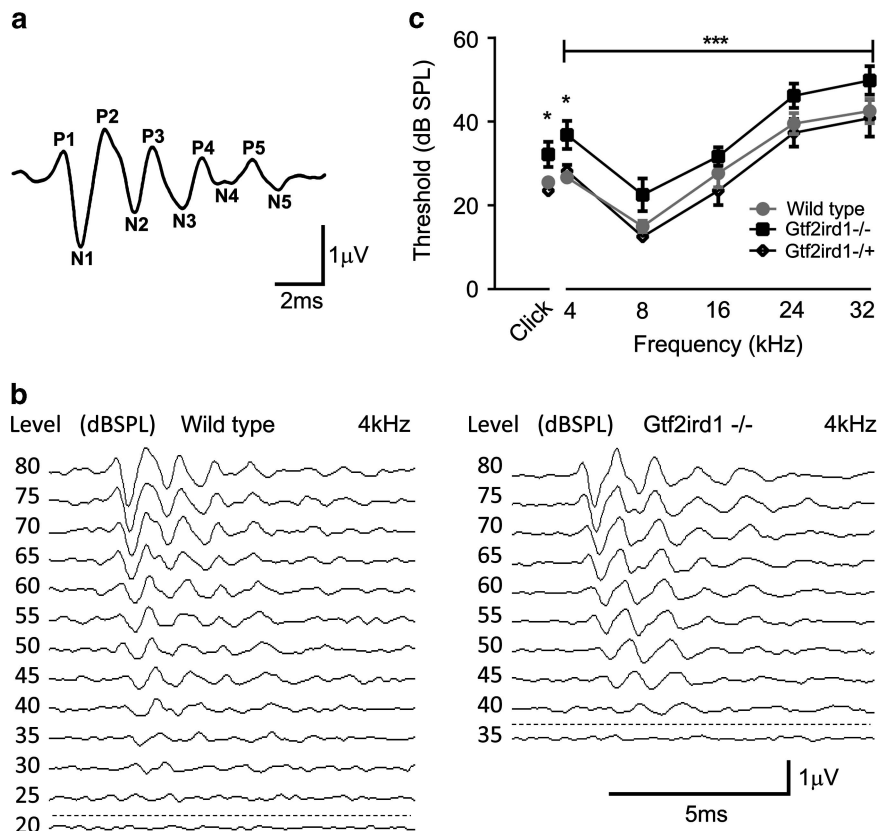


**Figure 3** Auditory brainstem response (ABR) threshold analysis. (a) ABR waveform response identified by peaks (P1–P5) and troughs (N1–N5). Peaks reflect sound-evoked responses generated by successive regions of the auditory pathway; example from 80 dB, 4 kHz stimulus in a wild-type mouse. (b) ABR waveform recordings over 10 ms to 4 kHz tone-pip stimuli from representative wild-type and *Gtf2ird1*<sup>-/-</sup> mice. Dashed line shows ABR thresholds. Interval was increased in 5 dB steps. (c) ABR thresholds to click and tone pips (4–32 kHz) in 8- to 10-week-old *Gtf2ird1*<sup>-/-</sup>, *Gtf2ird1*<sup>+/-</sup> and wild-type siblings ( $n=15$ /genotype; \*\*\* $P<0.001$ , two-way ANOVA on ranks; \* $P<0.05$ , Holm-Sidak multiple pairwise comparison between *Gtf2ird1*<sup>-/-</sup> and wild type). Data are expressed as means  $\pm$  SEM decibels sound pressure level (dB SPL).

### Recruitment and conduction of auditory nerve firing is not affected in *Gtf2ird1* knockout mice

By analysing the peak amplitudes and latencies of the ABR waveforms, effects on the recruitment and conduction elements of the auditory pathway can be assessed.<sup>26</sup> The peak amplitudes and latencies of P1-N1, P2-N2, P3-N3 and P4-N4 elements of the ABR waveform (Figure 3a) were analysed at 4 kHz (45 dB), where the greatest threshold difference was observed across the range of frequencies measured. This analysis showed that there were no significant differences in the latencies or growth functions of the first four peaks in the ABR between homozygous *Gtf2ird1*<sup>-/-</sup> and wild-type mice (Figure 4a and b, wild type  $n \geq 14$ ; *Gtf2ird1*<sup>-/-</sup>  $n \geq 11$ ;  $P=0.12$  via two-way ANOVA on ranks for 3A;  $P=0.41$  for peak I,  $P=0.48$  for peak II,  $P=0.15$  for peak III and  $P=0.08$  for peak IV via Holm-Sidak pairwise comparisons for Figure 4b). N1-P2 amplitude at 4 kHz also did not show significant difference (Figure 4c, wild-type  $n=13$ ; *Gtf2ird1*<sup>-/-</sup>  $n=6$ ;  $P=0.36$  via two-way ANOVA on ranks).

### *Gtf2ird1* null mice exhibit moderate loss of outer hair cell function

DPOAEs are generated by the reverse transduction cochlear micro-mechanics initiated by the outer hair cell, which changes its cell height and amplifies basilar membrane movement in response to the receptor potential generated by (forward) sound transduction. Two pure tones of close frequency range (1:1.25) and equal intensity are presented to the ear simultaneously and an 'echo' generated by the electromotility of the outer hair cells is detected by a sensitive microphone as DPOAE. The cubic QUOTE distortion products were analysed for threshold screening in *Gtf2ird1*<sup>-/-</sup> and *Gtf2ird1*<sup>+/-</sup> versus wild-type littermates. Thresholds were significantly higher across all tested frequencies in the *Gtf2ird1*<sup>-/-</sup> mice (Figure 5, ANOVA on ranks  $P < 0.01$ , Holm-Sidak all pairwise comparisons, comparing *Gtf2ird1*<sup>-/-</sup> and wild type: 8 kHz  $P=0.0006$ ; 12 kHz  $P=0.0025$ ; 16 kHz  $P=0.015$ ; 24 kHz  $P=0.053$ ; 32 kHz  $P=0.015$ ). The DPOAE threshold differences across all of the tested frequencies resemble the ABR results, where the strongest threshold difference was apparent at 8–16 kHz (average increase in DPOAE threshold in *Gtf2ird1*<sup>-/-</sup> mice: 8 kHz = 19.02 dB; 12 kHz = 15.52 dB; 16 kHz = 13.67 dB; 24 kHz = 8.59 dB; 32 kHz = 11.17 dB).

### DPOAE input/output functions in *Gtf2ird1*<sup>-/-</sup> mice show amplitude reductions at higher levels of sound

The input/output growth functions at 8, 12 and 32 kHz were analysed to examine the strength of cochlear sound transduction contributed by the outer hair cells. Growth function analysis of the cubic DPOAEs showed a significant roll-off on the progressive increase in amplitude of the cubic (DPOAE) in *Gtf2ird1*<sup>-/-</sup> compared with wild-type mice (Figure 6).

## DISCUSSION

This study demonstrates that 8 to 10-week-old *Gtf2ird1* knockout mice have a mild hypoacusis by ABR analysis, which is evident in the elevated threshold. However, analysis of the ABR waveforms suggests that there is no afferent conduction defect that might indicate a neural impairment of the cochlear nerve or subsequent elements of the brainstem auditory pathway. Analysis of *Gtf2ird1* expression in the cochlea demonstrated very high expression in the spiral ganglion, which is mainly composed of the cell bodies of afferent bipolar neurons. Spiral ganglion neurons are the first neurons in the auditory system to fire an action potential, and supply all the auditory input to the brain. Their dendrites make synaptic contact with the base of hair cells, and their axons are bundled together to form the auditory portion of the eighth cranial nerve. Detection of an alteration in the

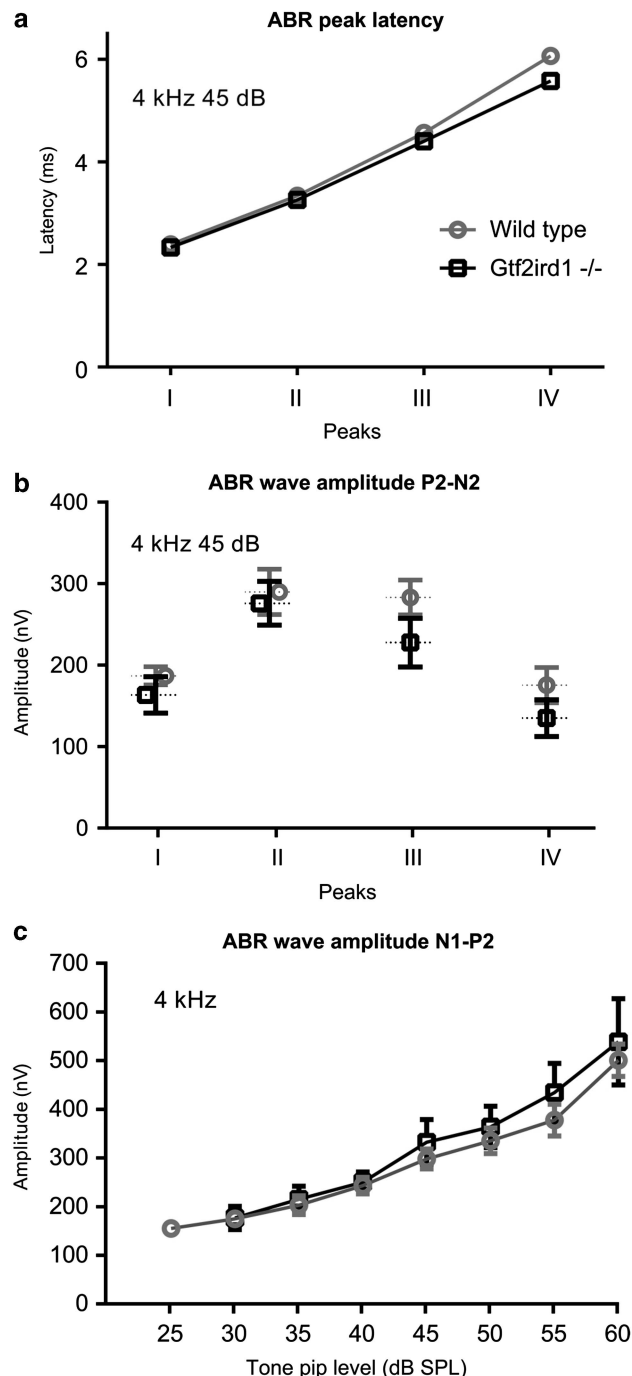


**Figure 4** ABR growth functions. (a) ABR input/output (I/O) functions for latency between peaks I to IV at 4 kHz in each genotype were equivalent. (b) Peak amplitudes at 4 kHz (45 dB,  $n=11$ ) measures auditory nerve conduction and recruitment. Despite genotype differences in thresholds, ABR peak latency and amplitude were similar. (c) Amplitude measurements of N1-P2, which corresponds to the auditory relay between the cochlear nerve and the brainstem, at 4 kHz from 25 to 60 dB (minimum  $n=6$ ). No significant difference was found between genotype, indicating a normal conduction and recruitment of auditory pathways in *Gtf2ird1*<sup>-/-</sup> mice ( $P > 0.05$ , ANOVA on ranks;  $P > 0.05$  Holm-Sidak multiple pairwise comparison). Data are expressed as means  $\pm$  SEM decibels sound pressure level (dB SPL).

conduction properties of these cells, or neurons comprising subsequent elements of the auditory pathway, may have provided a potential explanation for the auditory allodynia found in WBS. But if loss of the GTF2IRD1 protein impacts on these nerve cells, it has either had no effect on their conduction properties in this assay system or functional compensation has developed.

Analysis of DPOAE revealed that *Gtf2ird1* knockout mice showed a significant increase in thresholds, averaging 14 dB across the 8–32 kHz spectrum and with a greater difference at 8–16 kHz where hearing sensitivity is higher in the mouse. These data suggest that there is a defect in the cochlear amplifier associated with the outer hair cells and the extent of the difference is sufficient to explain the abnormality of the auditory threshold found in the ABR.

Analysis of the DPOAE input/output curve of the knockout mice shows a progressive roll off, in comparison with the wild-type curve, suggesting reduced outer hair cell amplification. This pattern is similar to what has been reported before in a mouse model of ageing.<sup>27</sup> However, mice were young at the time of testing (8–10 weeks) and genotypes were caged together under high-quality barrier conditions, thus making it unlikely that the hearing defect is due to secondary effects such as premature ageing, infections or environmental differences. Although we have reported that these mice have a craniofacial

defect,<sup>28</sup> analysis of skulls using micro-CT has failed to detect any changes in the dimensions or shape of the hard tissues and the defect appears to be restricted to the thickness of the epidermis overlying the nose and lip regions (Canales *et al*, unpublished). In addition, visual inspection indicated normal external auditory canals in the *Gtf2ird1*<sup>-/-</sup> mice. Thus, it is also unlikely that these hearing defects can be attributed to a developmental anomaly of the hearing apparatus as part of the craniofacial gestalt. The extent of the SNHL is not large enough to suggest the likelihood of a detectable change in cochlear structure and our histological observations support this view. The balance of data suggests that the principal defect resides within the function of the outer hair cells and this is most likely caused by a molecular defect either within these cells or by a dysfunction within the other *Gtf2ird1*-expressing cell types within the cochlea that contribute to the driving force for sound transduction, or the regulation of cochlear mechanics.

*Gtf2ird1* expression was mapped to the outer hair cells as well as a number of the closely associated supporting cell lineages within the organ of Corti and the interdental cells of the spiral limbus. The interdental cells have a role in the deposition of the tectorial membrane and deficits in the production of key structural proteins by these cells, such as CEACAM16, can lead to SNHL.<sup>29</sup> Similarly, Pillar cells and Deiters' cells create a rigid scaffold made of actin and microtubule bundles that support and surround the outer hair cells and facilitate an appropriate level of mechanical loading. These cells have been shown to be linked to the overall electromotility of the outer hair cell units, which can be impaired by the loss of the gap junction protein connexin 26, leading to SNHL.<sup>30</sup> The function of the outer hair cells is also dependent on a very high endocochlear potential (+95 mV), which is largely generated by the action of the marginal cells of the stria vascularis, which pump K<sup>+</sup> ions into the endolymph of the scala media and a passive outflow of K<sup>+</sup> through the organ of Corti and Reissner's membrane.<sup>31</sup> A large and prolonged drop in endocochlear potential is known to impair the mechanical sensitivity of the cochlea.<sup>31</sup> As the marginal cells of the stria vascularis, Reissner's membrane and several cell types within the organ of Corti were shown to express *Gtf2ird1*, it is possible that a dysfunction in these cells could contribute to the observed impairment of the cochlear amplifier through a disturbance to this strong ionic gradient.

The defect detected in the *Gtf2ird1* knockout mice bears a strong similarity to that observed in WBS patients, in that the dysfunction can be most easily detected early in DPOAE measurements.<sup>15–18</sup> However, there is no evidence in our mice of a mechanism within the auditory signal processing pathway that might explain the auditory allodynia in WBS patients.<sup>32</sup> It is possible that this phenomenon results from

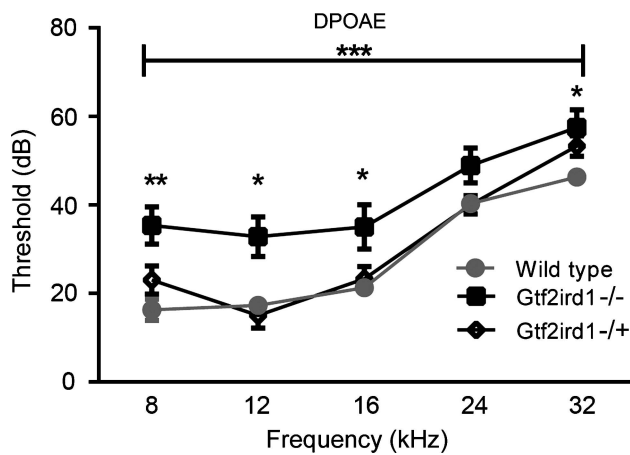


**Figure 5** Distortion products otoacoustic emission (DPOAE) thresholds. Cubic <sub>2F1-F2</sub> DPOAE in 8- to 10-week-old *Gtf2ird1*<sup>-/-</sup>, *Gtf2ird1*<sup>-/+</sup> and wild-type controls mice responding to 8–32 kHz puretone stimuli ( $n=15$  for each genotype; \*\*\* $P<0.001$ ; \*\* $P<0.001$ ; \* $P<0.05$ ). Data are expressed as means  $\pm$  SEM.

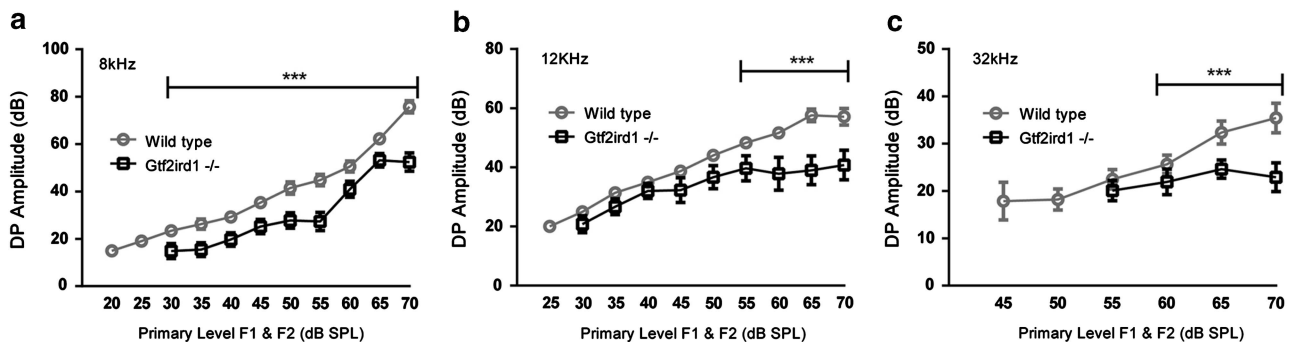


**Figure 6** DPOAE growth function. Input/output growth function analysis of cubic DPOAEs for wild-type and *Gtf2ird1*<sup>-/-</sup> littermates at (a) 8 kHz, (b) 12 kHz and (c) 32 kHz characterises the gain of outer hair cell reverse transduction reflecting cochlear amplifier sensitivity (\*\*\* $P<0.001$ ; two-way ANOVA on ranks; min  $n=9$  for wild type at 32 kHz; min  $n=7$  for *Gtf2ird1*<sup>-/-</sup> at 8, 12 and 32 kHz; max  $n=15$  at 8 kHz for wild type; max  $n=13$  at 8 kHz for *Gtf2ird1*<sup>-/-</sup>). Data are expressed as means  $\pm$  SEM.



events within the central nervous system beyond the capability of the ABR analysis to detect. It is also unclear to what extent the auditory allodynia is bound up with anticipatory anxiety and the polarisation of affective response to different types of auditory stimulus<sup>32</sup> that clearly has elements of emotional processing and anxiety control in addition to any mechanistic dysfunction of hearing.

Although the expression analysis provides some candidate cell types and potential mechanistic causes, what molecular events would underpin such a change in cell phenotype? Some GTF2IRD1 candidate gene targets have been identified by direct binding to enhancer elements within the developmental genes *Hoxc8*<sup>33</sup> and *Goosecoid*<sup>34</sup> and the skeletal muscle-specific *Troponin I slow*<sup>35</sup> or by microarray detection of differential gene regulation in a *Gtf2ird1* overexpression system.<sup>28</sup> However, an analysis of mRNA from *Gtf2ird1* knockout brain samples failed to identify evidence of any specific gene targets.<sup>28</sup> At this early stage, much of the basic information on how this protein operates is missing and suggests that the function is complex and cell context-dependent. Therefore, it is not possible to make realistic testable predictions of altered protein abundance that could be analysed in the cochlea of the knockout mice. Furthermore, as discussed above, there are multiple cell types within the cochlea that express *Gtf2ird1* and loss of the protein in any of these cells could cause the defect in the amplifier function. Progress in the understanding of the specific nature of the cochlear defect will have to await either a clearer understanding of the cell type that is primarily responsible and/or the molecular function of the GTF2IRD1 protein.

In conclusion, these data indicate a role for GTF2IRD1 in the hypoacusis of WBS patients and does not rule out a potential contribution to the auditory allodynia, which could be part of a central defect that cannot be assessed by the assays presented. No significant hearing defect was found in the heterozygous knockout animals, suggesting that GTF2IRD1 insufficiency is not enough to explain all of the hypoacusis in WBS. Additional separate hearing defects resulting from the reduction in other WBS gene products (eg, ELN, LIMK1, FZD9 and STX1A) may combine to form the whole. Alternatively, interactions at the molecular level may cause synergistic epistasis that enhances the severity of GTF2IRD1 hemizyosity when set within the context of the entire deletion. For example, the combined loss of GTF2IRD1 and GTF2I may enhance the severity of the phenotypes they generate to more than just an additive degree as evidence suggests that they share overlapping molecular functions.<sup>35</sup> Addressing these more complex questions will necessitate the interbreeding of mice carrying separate monogenic mutations.

## CONFLICT OF INTEREST

The authors declare no conflict of interest.

## ACKNOWLEDGEMENTS

We are grateful for the technical support of Dr Jennie Cederholm and Dr Kristina Froud in the Translational Neuroscience Facility at UNSW Australia. This work was supported by the National Health and Medical Research Council of Australia (Project Grant 1049639). Cesar Canales is a recipient of a CONICYT Becas-Chile scholarship (#72101076).

- 1 Stromme P, Bjornstad PG, Ramstad K. Prevalence estimation of Williams syndrome. *J Child Neural* 2002; **17**: 269–271.
- 2 Osborne LR, Mervis CB. Rearrangements of the Williams-Beuren syndrome locus: molecular basis and implications for speech and language development. *Expert Rev Mol Med* 2007; **9**: 1–16.
- 3 Jarvinen A, Korenberg JR, Bellugi U. The social phenotype of Williams syndrome. *Curr Opin Neurobiol* 2013; **23**: 414–422.

- 4 Antonell A, Del Campo M, Magano LF *et al*: Partial 7q11.23 deletions further implicate GTF2I and GTF2IRD1 as the main genes responsible for the Williams-Beuren syndrome neurocognitive profile. *J Med Genet* 2010; **47**: 312–320.
- 5 Jackson TA, Taylor HE, Sharma D, Desiderio S, Danoff SK. Vascular endothelial growth factor receptor-2: counter-regulation by the transcription factors, TFII-I and TFII-IRD1. *J Biol Chem* 2005; **280**: 29856–29863.
- 6 Palmer SJ, Taylor KM, Santucci N *et al*: GTF2IRD2 from the Williams-Beuren critical region encodes a mobile-element-derived fusion protein that antagonizes the action of its related family members. *J Cell Sci* 2013; **125**: 5040–5050.
- 7 Tantin D, Tussie-Luna MI, Roy AL, Sharp PA. Regulation of immunoglobulin promoter activity by TFII-I class transcription factor. *J Biol Chem* 2004; **279**: 5460–5469.
- 8 Howard ML, Palmer SJ, Taylor KM *et al*: Mutation of *Gtf2ird1* from the Williams-Beuren syndrome critical region results in facial dysplasia, motor dysfunction, and altered vocalisations. *Neurobiol Dis* 2012; **45**: 913–922.
- 9 Schneider T, Skitt Z, Liu YW *et al*: Anxious, hypoactive phenotype combined with motor deficits in *Gtf2ird1* null mouse model relevant to Williams syndrome. *Behav Brain Res* 2012; **233**: 458–473.
- 10 Tassabehji M, Hammond P, Kamiloff-Smith A *et al*: GTF2IRD1 in craniofacial development of humans and mice. *Science* 2005; **310**: 1184–1187.
- 11 Young EJ, Lipina T, Tam E *et al*: Reduced fear and aggression and altered serotonin metabolism in *Gtf2ird1*-targeted mice. *Genes Brain Behav* 2008; **7**: 224–234.
- 12 Levitin DJ, Menon V, Schmitt JE *et al*: Neural correlates of auditory perception in Williams syndrome: an fMRI study. *Neuroimage* 2003; **18**: 74–82.
- 13 Cherniske EM, Carpenter TO, Klaiman C *et al*: Multisystem study of 20 older adults with Williams syndrome. *Am J Med Genet A* 2004; **131**: 255–264.
- 14 Marler JA, Eifenbein JL, Ryals BM, Urban Z, Netzloff ML. Sensorineural hearing loss in children and adults with Williams syndrome. *Am J Med Genet A* 2005; **138**: 318–327.
- 15 Barozzi S, Soi D, Comiotto E *et al*: Audiological findings in Williams syndrome: a study of 69 patients. *Am J Med Genet A* 2012; **158A**: 759–771.
- 16 Barozzi S, Soi D, Spreafico E *et al*: Audiological follow-up of 24 patients affected by Williams syndrome. *Eur J Med Genet* 2013; **56**: 490–496.
- 17 Marler JA, Sitovsky JL, Mervis CB, Kistler DJ, Wightman FL. Auditory function and hearing loss in children and adults with Williams syndrome: cochlear impairment in individuals with otherwise normal hearing. *Am J Med Genet C Semin Med Genet* 2010; **154C**: 249–265.
- 18 Paglialonga A, Barozzi S, Brambilla D *et al*: Cochlear active mechanisms in young normal-hearing subjects affected by Williams syndrome: time-frequency analysis of otoacoustic emissions. *Hear Res* 2011; **272**: 157–167.
- 19 Matsumoto N, Kitani R, Kalinec F. Linking LIMK1 deficiency to hyperacusis and progressive hearing loss in individuals with Williams syndrome. *Commun Integr Biol* 2011; **4**: 208–210.
- 20 Shah SM, Kang YJ, Christensen BL, Feng AS, Kollmar R. Expression of Wnt receptors in adult spiral ganglion neurons: frizzled 9 localization at growth cones of regenerating neurites. *Neuroscience* 2009; **164**: 478–487.
- 21 Safieddine N, Wenthold RJ. SNARE complex at the ribbon synapses of cochlear hair cells: analysis of synaptic vesicle- and synaptic membrane-associated proteins. *Eur J Neurosci* 1999; **11**: 803–812.
- 22 Lucena J, Pezzi S, Aso E *et al*: Essential role of the N-terminal region of TFII-I in viability and behavior. *BMC Med Genet* 2010; **11**: 61.
- 23 Palmer SJ, Santucci N, Widagdo J *et al*: Negative Autoregulation of GTF2IRD1 in Williams-Beuren Syndrome via a Novel DNA Binding Mechanism. *J Biol Chem* 2010; **285**: 4715–4724.
- 24 Palmer SJ, Tay ESE, Santucci N *et al*: Expression of *Gtf2ird1*, the Williams syndrome-associated gene, during mouse development. *Gene Expr Patterns* 2007; **7**: 396–404.
- 25 Wong ACY, Birnbaumer L, Housley GD. Canonical transient receptor potential channel subtype 3-mediated hair cell Ca<sup>2+</sup>-entry regulates sound transduction and auditory neurotransmission. *Eur J Neurosci* 2013; **37**: 1478–1486.
- 26 Legatt AD. Mechanisms of intraoperative brainstem auditory evoked potential changes. *J Clin Neurophysiol* 2002; **19**: 396–408.
- 27 Parham K. Distortion product otoacoustic emissions in the C57BL/6J mouse model of age-related hearing loss. *Hear Res* 1997; **112**: 216–234.
- 28 O'Leary J, Osborne LR. Global analysis of gene expression in the developing brain of *Gtf2ird1* knockout mice. *PLoS One* 2011; **6**: e23868.
- 29 Kammerer R, Ruttiger L, Riesenberger R *et al*: Loss of mammal-specific tectorial membrane component carcinoembryonic antigen cell adhesion molecule 16 (CEACAM16) leads to hearing impairment at low and high frequencies. *J Biol Chem* 2012; **287**: 21584–21598.
- 30 Zhu Y, Liang C, Chen J, Zong L, Chen GD, Zhao HB. Active cochlear amplification is dependent on supporting cell gap junctions. *Nat Commun* 2013; **4**: 1786.
- 31 Patuzzi R: Ion flow in cochlear hair cells and the regulation of hearing sensitivity. *Hear Res* 2011; **280**: 3–20.
- 32 Levitin DJ, Cole K, Lincoln A, Bellugi U. Aversion, awareness, and attraction: investigating claims of hyperacusis in the Williams syndrome phenotype. *J Child Psychol Psychiatry* 2005; **46**: 514–523.
- 33 Bayarsaihan D, Ruddle FH. Isolation and characterization of BEN, a member of the TFII-I family of DNA-binding proteins containing distinct helix-loop-helix domains. *Proc Natl Acad Sci USA* 2000; **97**: 7342–7347.
- 34 Ring C, Ogata S, Meek J *et al*: The role of a Williams-Beuren syndrome-associated helix-loop-helix domain-containing transcription factor in activin/nodal signaling. *Genes Dev* 2002; **16**: 820–835.
- 35 O'Mahoney JV, Guven KL, Lin J *et al*: Identification of a novel slow-muscle-fiber enhancer binding protein, MusTRD1. *Mol Cell Biol* 1998; **18**: 6641–6652.